Surgical and Radiologic Anatomy (2022) 44:535–542
https://doi.org/10.1007/s00276-022-02916-9

ORIGINAL ARTICLE

Radiological evaluation of maxillary artery and descending palatine artery in the pterygopalatine fossa by 3D rotational angiography

Ibrahim Ilker OZ[1] · **Ahmet Aydogdu**[2] · **Temel Fatih Yilmaz**[1]

Received: 10 December 2021 / Accepted: 21 February 2022 / Published online: 7 March 2022

Abstract

Purpose The aim of this study is to evaluate the branching patterns and topographical features of the third part of the maxillary artery (t-MA) and descending palatine artery (DPA) by 3-Dimensional Rotational Angiography (3DRA) images and to define the radiological classification of their variations, based upon the previous cadaveric studies and a review of the literature.

Method This study was conducted from May 2020 through June 2021. All consecutive adult patients who were examined with 3D-RA were enrolled in the study. The morphological evaluations and measurements of t-MA, DPA and their branches were made on maximum intensity projection images with 10–20 mm slice thickness.

Results Eighty-five hemifaces, including 58 females and 45 right sides, were evaluated. The diameter of the t-MA was measured as 1.73 ± 0.30 mm. The most common pattern of the t-MA according to its course was loop type (63/85, 74.1%) and according to branching pattern was Type Ib (29/85, 34.1%). The mean diameter of DPA was 1.19 ± 0.20 mm. The DPA presented as a single trunk in 11/85 cases. Type II, which was defined as one lesser palatine artery originating from distal-DPA, was the most common morphological variation (51.8%).

Conclusions 3DRA imaging provides valuable information for vascular anatomical studies. The most common morphological variation related to t-MA, DPA is the distal branching pattern.

Keywords Maxillary artery · Descending palatine artery · Variation · Rotational angiography · Cone-beam computer tomography

Introduction

The third part of the maxillary artery (t-MA) is a terminal branch located inside the pterygopalatine fossa (PPF) [7, 12, 24]. The t-MA and branches are very vulnerable to trauma during endoscopic nasal and maxillofacial surgeries like Le Fort I osteotomy or posterior epistaxis and regional anaesthesia procedures because of their position in the PPF and the greater palatine canal (GPC) [2, 3, 7, 26, 27]. Knowing and understanding the anatomical structure of the MA and its branches will prevent complications that may occur during procedures performed in this region.

The descending palatine artery (DPA) is one of the terminal branches and the most common source of major bleeding during Le Fort I osteotomy [2]. Once it emerges from the greater palatine foramen, the DPA continues as the greater palatine artery (GPA) and supplies the hard palate [12, 17, 24]. A side branch of the DPA is the lesser palatine artery (LPA), which descends within the GPC, or the lesser palatine canal (LPC). Furthermore, some authors reported that the inferior turbinate artery (ITA) is a branch of the DPA [13, 23]. The GPC and LPC communicate with the oral cavity, and this makes them important and vital for all interventional procedures related to this area and their respective nerves and arteries [21].

✉ Ibrahim Ilker OZ
ilkeroz@yahoo.com

Ahmet Aydogdu
ahm0067@gmail.com

Temel Fatih Yilmaz
temelfatihyilmaz@gmail.com

[1] Faculty of Medicine, Department of Radiology Topkapı, Bezmialem Vakif University, Adnan Menderes Blv. Fatih, 34093 İstanbul, Turkey

[2] Faculty of Dentistry, Department of Periodontology Topkapı, Bezmialem Vakif University, Adnan Menderes Blv. Fatih, 34093 İstanbul, Turkey

The morphological presentation of t-MA can be variable, and the Morton and Khan classification is most-commonly used system in cadaver studies [3, 7, 12, 16, 26]. This classification is based on sphenopalatine artery (SPA)-DPA bifurcation patterns and there are different interpretations of the classification in several studies [3, 7, 12]. For the classification of DPA, very limited studies focused on this issue and there is no consensus about the classification [7, 26]. Moreover, the classifications of t-MA and DPA were made during cadaver studies and they involved limited study populations as expected [3, 7, 11, 12, 16, 23, 26, 28]. There are very few radiological studies that evaluated the t-MA and branches, and the majority of these are Cone Beam Computer Tomography (CBCT) studies without contrast enhancement [5, 15, 19]. Radiological classification of the t-MA and branches has not been defined in these studies due to the technical issues of imaging methods.

Three-dimensional rotational angiography (3DRA) is a novel imaging method that combines the most important advantages of conventional angiography and CT. 3DRA with high resolution, thin section extending down to the submillimetre level allows the evaluation of distal arteries and their relationships with bone and soft tissues. Furthermore, one of the most important benefits of radiology over cadaver study is the inspection of *in vivo* anatomy. In the cadaver study, the shape and texture of organs and tissues necessarily differ from their premortal state. In contrast, radiological studies are obtained in patients who are still living, and whose organs and tissues manifest their native *in vivo* appearances. Besides, the knowledge about medical records and comorbidities of the patients is another advantage of radiological studies. In the English medical literature, no radiologic study was found in which t-MA and DPA were assessed with the advantages of this imaging method.

The aim of this study is to evaluate the branching patterns and topographical features of the t-MA and DPA by 3DRA images and to define the radiological classification of their variations, based upon the previous cadaveric studies and a review of the literature.

Material and methods

Population

From May 2020 through June 2021, all consecutive adult patients examined with cerebral or carotid artery digital subtraction angiography imaging with unilateral or bilateral 3D-RA via common carotid artery injection were reviewed for enrolment. Patients who had dentofacial deformities and external carotid artery stenosis more than 70% or total occlusion were excluded from the study. Sixty consecutive patients (24 males and 36 females; mean age: 50.5 ± 13.85 years) abiding by the inclusion criteria were enrolled. Twenty-five patients were bilaterally imaged, and in total 85 hemifaces were examined with 3D-RA images. This cross-sectional study was approved by our institutional ethics committee and all individuals provided written informed consent to participate.

3D-RA and CBCT image protocols

The 3D-RA and flat-panel CBCT data were acquired using a monoplane flat-panel angiography system (Allura Xper FD20, Philips Medical Systems, the Netherlands). The "Cerebral Prop Scan" acquisition protocol with manufacturer's default settings was used. Raw data were acquired with a diagnostic catheter located in the common carotid artery. Contrast medium (300 mg I/mL) was infused with a rate of 4 mL/s for 6 s (total volume of 24 mL) with a 2-s imaging delay.

After post processing of raw data using Allura 3D-RA 6.4.6 and XperCT Dual 3.2.6 (Philips Medical Systems Netherland B.V. The Netherlands) on a workstation, very high spatial resolution CBCT reconstructions with 0.14–0.36 mm slice thickness were obtained.

Image analysis

For each patient, CBCT image analysis was completed by two radiologists and one periodontologist with consensus using Allura 3D-RA 6.4.6 on a workstation. The reviewers could manipulate the images to optimize the visualization of vascular structures for the evaluation of morphological findings. The measurements were made using the same anatomical landmarks for standardization on the multiplanar reconstruction screen. For standardization, the line parallel the incisive fossa and the posterior nasal spine was selected on the axial images. On sagittal images, the second line was selected parallel to the nasal line. Finally, the line parallel to the hard palate was chosen on coronal images.

The morphological evaluations and measurements of t-MA were made on coronal maximum intensity projection images with 10–20 mm slice thickness. The t-MA was classified into 3 patterns according to its course in the PPF as described by Kwak et al. [12] (Fig. 1). The variations of t-MA also comprised SPA-DPA bifurcation angle degree, which was defined with the modification of the Morton and Khan classification [3, 12].

- Type I; angulation (0–30°) (Type M, Morton and Khan). The subgroups were defined according to the location of the bifurcation. Type Ia was proximal and Type Ib was distal (Fig. 2a–b).
- Type II; angulation (30–120°). The subgroups of Type II were defined according to the dominant branch of

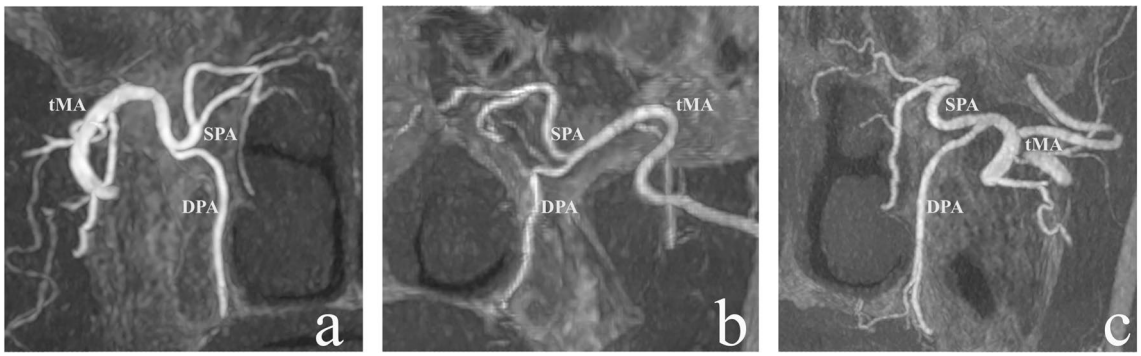

Fig. 1 On coronal maximum intensity projection image, the third part of the maxillary artery was divided into 3 morphological categories as looped (**a**), straight (**b**) and bifurcated (**c**) pattern according to its course that defined by Kwak classification. The most frequent MA coursing pattern was Loop form with 74.1%. Straight and Bifurcated forms were seen at 16.5% and 9.4% respectively

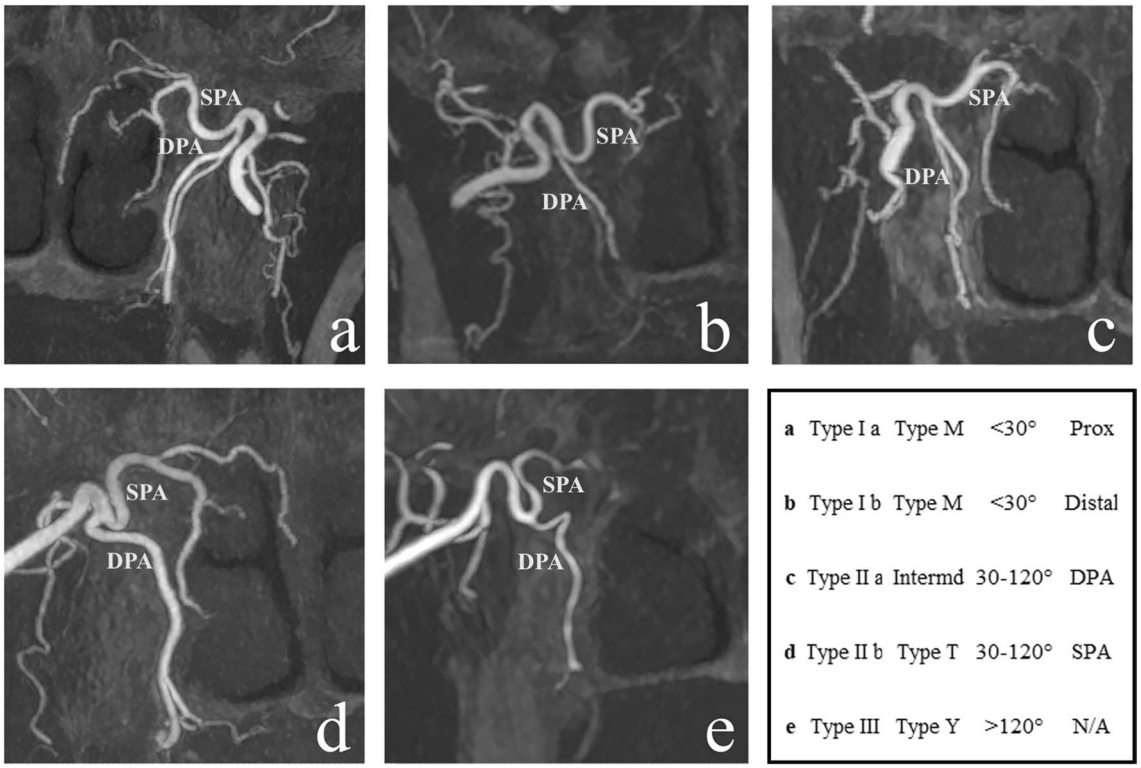

Fig. 2 The third part of the maxillary artery was divided into 3 morphological classification and their subgroups were defined according to branching of descending palatine artery (DPA) and sphenopalatine artery (SPA) by adaptation and modification of Morton and Khan classification on coronal maximum intensity projection image. Type I: modified from Type M (Morton and Khan), the angulation between SPA and DPA is 0–30°. The subgroups were defined according to the location of the bifurcation. Type Ia was proximal (**a**) and Type Ib was distal (**b**). Type II: modified from Type T and Type intermediate (Morton and Khan), the angulation between SPA and DPA is 30–120°. The subgroups of Type II were defined according to the dominant branch of bifurcation. If SPA was the terminal branch and larger than DPA, it was Type IIa (Type T) (**c**) and otherwise, it was Type IIb (Type intermediate) (**d**). Type III; modified from Type Y (Morton and Khan), the angulation between SPA and DPA is > 120° (**e**)

bifurcation. If SPA was the terminal branch and larger than DPA, it was Type IIa (Type T, Morton and Khan) (Fig. 2c) and otherwise, it was Type IIb (Type intermediate, Morton and Khan) (Fig. 2d).

- Type III; angulation (> 120°) (Type Y, Morton and Khan) (Fig. 2e)

The morphological classification of the DPA was evaluated according to the branching of the LPA from DPA, ignoring the MA (Fig. 3a–d). The DPA was identified as proximal DPA (p-DPA) and distal DPA (d-DPA) according to GPC.

- Type I; Single DPA
- Type II; One LPA originates from p-DPA
- Type III; One LPA originates from d-DPA
- Type IV; Two or more LPAs originate from DPA

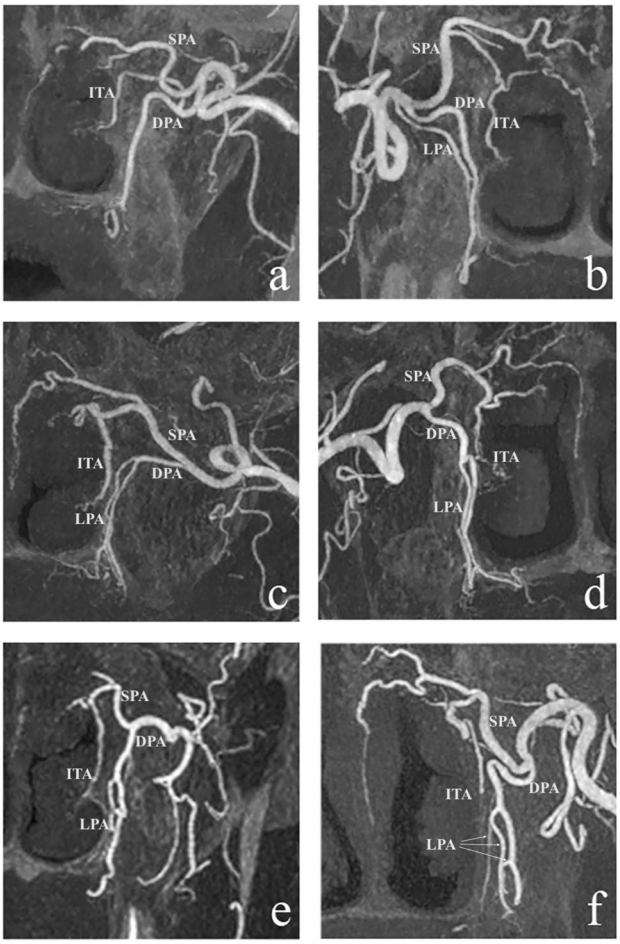

Fig. 3 On coronal maximum intensity projection image, the morphological classification of the descending palatine artery (DPA) was assessed consistent with the branching of the lesser palatine artery (LPA). The morphological evaluation of LPA was classified as Type I originating from MA, Type II from DPA, Type III from both, ignoring the branching level, and Type IV no artery. Type I-DPA (Single DPA) with inferior tribunate artery originated from DPA and Type IV-LPA (**a**), Type I-DPA and Type I-LPA (**b**), Type II-DPA (One LPA originates from proximal-DPA) and Type II-LPA (**c**), Type III-DPA (One LPA originates from distal-DPA) and Type II-LPA (**d**), Type IV-DPA (Two or more LPAs originate from DPA) and Type II-LPA (**e**), Type IV-DPA, Two LPAs originate from DPA and one LPA from t-MA (Type IV-LPA) (**f**)

The morphological evaluation of LPA was classified as Type I originating from MA, Type II from DPA, Type III from both, ignoring the branching level, and Type IV no artery (Fig. 3).

On standardized axial images, (1) DPA diameter was measured inside the PPF at the level of the GPC entry, (2) LPA diameter was measured from the proximal part of the major LPA branch.

The LPC is posterior to the GPC, crosses the pyramidal process of the palatine bone and opens as the lesser palatine foramen (LPF) [25]. The number of LPC (nLPC) and LPF (nLPF) was determined on sagittal and axial images respectively (Fig. 4a–b).

The length of the maxillary sinus medial wall (l-GPC_PR) was measured from the piriform rim (PR) to the anterior wall of the GPC as described by Apinhasmit et. al. to simulate the lateral maxillary cut during Le Fort I osteotomy [2].

Statistical analysis

SPSS software (ver. 21.0 for Windows; SPSS Inc., Chicago, IL, USA) was used for statistical analysis. Descriptive statistics are given with mean, standard deviation, median, minimum and maximum values or with frequency and percent for continuous or qualitative variables respectively. The Shapiro Wilk test was used for the test of normality. The independent samples *t* test was used for two group comparisons of normally distributed variables. For non-normally distributed variables, the Kruskal–Wallis test was performed for independent group comparisons. The Bonferroni-corrected Mann–Whitney *U* test was used for post-hoc analysis. For all statistical comparisons, a p value below 0.05 was assumed to be statistically significant.

Results

A total of 85 adult hemifaces, including 58 females (68.2%) and 45 right sides (52.9%), were evaluated. The morphological classifications and diameters of the t-MA, DPA and LPA are given in Table 1. The diameter of the t-MA was measured as 1.73 ± 0.30 mm and had significant differences based on gender (male 1.86 ± 0.27 mm, female 1.67 ± 0.29 mm $p = 0.005$) and between Type I and Type II morphological classification of t-MA when subgroups were combined ($p = 0.004$). There was no significant difference with age, side, l-GPC_PR or the morphological pattern of the t-MA ($p = 0.07$, 0.87, 0.81, 0.16 and 0.33, respectively).

The most common pattern of the t-MA according to its course was loop type (63/85, 74.1%). No significant relationship was detected with age, gender, side and l-GPC_PR ($p = 0.09$, 0.72, 0.38 and 0.64, respectively).

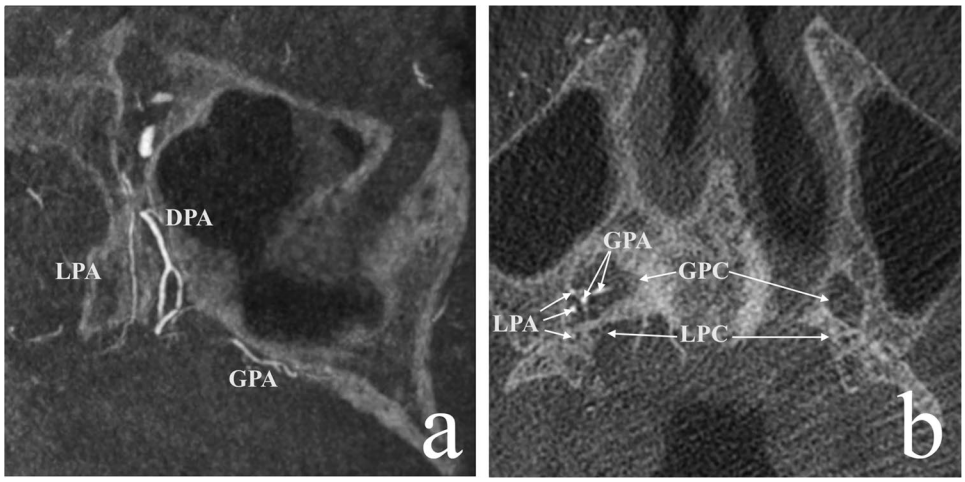

Fig. 4 On sagittal maximum intensity projection image (**a**), lesser palatine canal (LPC), and inside LPC, lesser palatine artery (LPA) was observed. Additionally, inside the greater palatine canal second LPA was branching from descending palatine artery. On axial images of the same case (**b**), LPC with LPA and concomitant lesser palatine foramen was seen, and on the left side of the patient 3 LPC were observed

Table 1 The morphological classifications and diameters of the third part of the maxillary artery, descending palatine artery and lesser palatine artery

Artery	Morphological classification	Frequency	Percentage (%)	Diameter (mm ± SD)
Maxillary artery (Morton[a])	Type Ia (Type M, proximal)	10	11.8	1.99 ± 0.30[ǂ §]
	Type Ib (Type M, distal)	29	34.1	1.79 ± 0.28[ǂ §]
	Type IIa (Type intermediate)	16	18.8	1.61 ± 0.28[ǂ ¥]
	Type IIb (Type T)	26	30.6	1.66 ± 0.28[ǂ ¥]
	Type III (Type Y)	4	4.7	1.50 ± 0.21[§ ¥]
Maxillary artery (Kwak[b])	Loop	63	74.1	1.72 ± 0.30
	Straight	14	16.5	1.83 ± 0.25
	Bifurcated	8	9.4	1.63 ± 0.34
Descending palatine artery	Type I	11	12.9	1.06 ± 0.24
	Type II	18	21.2	1.25 ± 0.18
	Type III	44	51.8	1.18 ± 0.20
	Type IV	12	14.1	1.2 ± 0.15
Lesser palatine artery	Type I	4	4.7	0.80 ± 0.14
	Type II	58	68.3	0.81 ± 0.17
	Type III	16	18.8	0.81 ± 0.21
	Type IV (absent)	7	8.2	–

[a]Classified according to modification of Morton and Khan Classification

[b] Classified according to t-MA course and branching pattern defined by Kwan et. al

[ǂ]Statistical difference between Type I and Type II ($p = 0.004$ǂ) Mann–Withney U test with Bonferroni adjustment (3 groups were evaluated)

[§]No statistical difference between Type I and Type III ($p = 0.04$§) / Type II and Type III ($p = 0.42$¥) Mann–Withney U test with Bonferroni adjustment (3 groups were evaluated)

The most common type of the t-MA according to branching pattern was Type Ib (29/85, 34.1%) and the second was Type IIb (26/85, 30.6%). No significant relationship was found with age, gender, side and l-GPC_PR ($p = 0.73$, 0.27, 0.65 and 0.87, respectively).

In all cases, DPA gave rise to GPA as the terminal branch. The mean diameter of DPA was 1.19 ± 0.20 mm and this had a significant relationship with gender (male:1.28 ± 0.19 mm, female:1.15 ± 0.19 mm $p = 0.005$). There was no significant relationship with age, side, l-GPC_PR, and classification of DPA ($p = 0.57$, 0.30, 0.93 and 0.45, respectively).

The DPA presented as a single trunk in 11/85 cases (12.9%, 7 cases, no LPA and 4 cases LPA originated from MA). Type II, which was defined as one LPA originating from d-DPA, was the most common morphological variation (44/85 cases—51.8%). It gave rise to three branches in 6/85 cases (7.1%). In 2 hemifaces (2.35%), one ITA originated from the DPA (Fig. 3a).

The mean diameter of LPA was 0.80 ± 0.18 mm and had no significant relationships with age, gender, side and the l-GPC_PR ($p = 0.07$, 0.37, 0.62 and 0.10, respectively). The number of LPA was found to range from 0 to 3; it was absent in 7/85 cases (8.2%), single in 49/85 (57.6%), double in 19/85 cases (22.4%), and triple in 10/85 cases (11.8%). No significance was found for relationships with age, sex, side and the diameter of LPA ($p = 0.08$, 0.48, 0.46 and 0.44, respectively).

LPC was found in 56.5% (48/85) of the hemifaces and 44.7% had one canal. All observed LPCs were posteromedial to the GPC, with no anterior LPC detected. LPC and LPA relationship and frequencies are given in Table 1. There was no significant relationship between the nLPC and age, gender, side, diameter of LPA, l-GPC_PR or morphological classification of LPA ($p = 0.06$, 0.18, 0.54, 0.87, 0.61 and 0.91, respectively).

The nLPF was ranged from 0 to 5. Two LPFs were most frequently observed in 26/85 cases (30.6%). No significant differences were found between nLPF and age, gender side, diameter of LPA, nLPA and nLPC, and l-GPC_PR ($p = 0,11$, 0,72, 0,43, 0.85, 0.30, 0.15 and 0.08, respectively).

The mean length of GPC_PR was measured as 40.66 ± 4.01 mm and it had a significant relationship with gender (male 40.77 ± 3.1 mm, female 40.61 ± 4.38 mm) ($p = 0.04$). There was no significant difference between l-GPC_PR and age for adult patients ($p = 0.18$).

Discussion

The classifications of t-MA and DPA were evaluated only in cadaver studies and there is no comparable data in radiology studies. The most important technical features that distinguish radiological studies from cadaver studies are that the range of values for angulation can be given, all these can be repeated for different observers and studies, *in vivo* evaluation and easy application. The use of MRP and 3D imaging methods allow maxillary artery classification to be performed in detail. Therefore, a new modified classification of t-MA and DPA was created by means of cadaveric studies.

Morphological classification and diameter of MA

Morton and Khan defined the morphological classification of the t-MA according to its overall contour in the PPF [16]. This overall contour was defined according to two parameters: the location and the angle of the DPA branching. According to these parameters, they defined "M" contour approaches at 0 degrees or the DPA branches proximally in the PPF, the "Y" contour approaches at 180 degrees or the DPA branches distally in the PPF, and the intermediate form is approximately 90 degrees or branching occurs between these extremes [16].

Choi & Park modified the classification of Morton & Khan and added the "T" contour for cases that had < 90 degrees between DPA and MA [7]. Furthermore, they could not classify 9.6% of cases because of the bifurcation location [7].

After the subtraction of bone structures, MIP images make it possible to evaluate the angulation and the location of vascular structures. This feature allowed radiological classification of t-MA within PPF. The "M" form was divided into two subgroups as proximal and distal because the narrow angle was measured on both sides. Therefore, the definitions of Morton & Khan (angulation and location) were combined for the "M" form. Another point is the attempt to overcome the grey zone between the "intermediate" and "T" form definitions by identifying the dominant artery.

In our study, Type 1b (Type M distal, 34.1%, 29/85) is the most common branching type of t-MA. Morton & Khan found the intermediate type (50%) was the most common in 30 serial cadavers dissections [16]. Choi & Park reported that the Y type was found in 4 (19.0%) cases, the intermediate in 7 (33.3%), the T type in 5 (23.8%), and the M type in 3 (14.3%) cadavers in 21 serial dissections [7]. Nevertheless, they classified 2 cases as other types (9.6%) [7]. In the study by Uysal et al., type "Y" was found in 50% (7/14) [28]. Kwak et al. reported that intermediate type was found in 36 cases in the largest cadaver dissection series (100 hemifaces) [12]. Assam et al. reported that the intermediate type was most common ($n = 9$, 53%), followed by M-type in 41% ($n = 7$) and no Y-types identified [3]. As a summary of the studies evaluating the SPA-DPA bifurcation pattern, the intermediate type was identified as the most common (33–53%) [3, 7, 12, 16]. The remaining pattern frequencies were highly variable [3, 7, 12, 16, 28]. We observed that type IIb (intermediate type) was the second most common type, with most bifurcations located in the distal part of the PPF.

The branching levels of the t-MA and DPA could not be optimized due to dissections via the transantral approach in cadaver studies, and insufficient section thickness or lack of contrast agent in previous radiological studies. This study showed that arterial branching at the PPF level is located distally. And this might increase the risk of vascular injury, especially in maxillary anesthetic implications for PPF via GPC. Additionally, because of the distal location of the bifurcation, both DPA and SPA are vulnerable during PPF Le Ford I procedure.

According to us, the different results of these studies are not explained only by ethnicity or population size. The visual evaluation of cases and deficiencies in the classification system of the MA in PPF may cause these different results. When the definition of intermediate type (approximately 90 degrees or branching occurs between M and Y) is also taken

into account, it is more understandable why it was the most common in previous studies.

We found that the diameter of t-MA and the length of GPC_PR were significantly thick and larger in males. Nevertheless, there was no relationship between the length of GPC_PR and the diameter of t-MA. Although we showed a relationship between the types and thicknesses of MA in contrast-enhanced examination, these sub-millimetric differences will not make a significant difference during a procedure involving the PPF in daily practice.

Morphological classification of DPA and LPA

Two studies focusing on morphological differences of the DPA in the PPF were identified [7, 26]. The definition of the DPA was accepted as the entry point into the greater palatine foramen (GPF), as described in previous studies [11, 24]. Nonetheless, Choi & Park accepted it up to the branching of LPA-GPA [7]. Choi & Park classified the DPA according to the branching location of GPA and LPA [7]. In this study, the most common in 95.2% of cases was short DPA that branched after 4–5 mm from MA. Toure reported that the DPA had three types of morphological variation [26]. Similarly, Toure divided the DPA according to branching and defined a single artery in 6 of 24 cases, a GPA and LPA called classical type in 17 of 24 cases and more than two arteries in one case.

In our study, the definition of DPA and previous studies were evaluated together and classified according to the number and branching of LPA. Type III (51.8%) was the most common. These results are similar to the previous studies [7, 26].

We found three LPAs in 10 hemifaces (11.8%) and in 7 cases (8.2%) LPA was not detected. Complications such as bleeding (2%) and wound dehiscence (2%) observed in the uvulopalatal flap procedure are highly likely to be seen in these patient groups, although it is currently not possible to detect these variations before the procedure [18].

As in previous studies, we did not find a significant relationship between the demographic features and cephalometric measurements [2, 27]. In our study, DPA was found in all GPC, 56.5% of the cases had LPC, and 93.75% (45/48) had LPA in the canal. In all cases with LPC, the canal was observed posteriorly to the GPC. This result, like other studies, shows that non-enhanced CT imaging is a suitable and cost-effective imaging method to recognize the anatomy of the PPF and the location of DPA before Le Fort I osteotomy [2, 27].

Morphological evaluation of LPF and LPC

nLPF was explored in several studies and maximum nLPF ranged from 3 to 5 [5, 6, 8–10]. Like previous studies from the same region, we observed that the maximum nLPF was 5 [5, 6]. NLPFs were frequently found to be two (26 cases-30.6%) and the absence of LPF was observed in 4 cases (4.7%) in the present study.

There are limited studies about LPC [4, 5, 15]. In the English medical literature, there is no study about the number of canals and arteries passing through it. In this study, there was no duct in 37/85 cases (43.5%), while a single duct was detected in 38/85 cases (44.7%). Arterial structure was not observed in the LPC in 3 (3.5%) of the cases with a single duct. While LPA was not detected at all in one of these cases, LPA was observed in the GPC in 2 of them. If the presence of LPC was shown on CT, it can be considered as passing the LPA.

ITA as a branch of DPA

The ITA is reported to be a branch of the DPA [1, 13, 20, 23]. Some authors reported no contribution from the DPA to the ITA [14, 22]. Lee et al. stated that it was a branch off the DPA in 1/50 Korean adult cadaver heads (2%) [13]. Orhan et al. indicated that a branch from the DTA merged with the ITA in 3/21 hemifaces (15%) [20]. Al-Shouk et al. reported that in the 2/40 hemifaces, the IT had blood supply from DPA or it came solely from a branch of DPA [1]. In our study, IT artery was observed as a branch of DPA in 2/85 cases (2.35%). Scott et al. stated that in 13/24 hemifaces (54.2%), the ITA was found to arise entirely as a branch of the DPA [23]. In this study, all dissections were performed endoscopically and evaluated by a single observer. These may be reasons for the high ratio of IT arteries branching from DPA.

In cases of recurrent posterior epistaxis, the presence of accessory localized IT might be considered and treatment options for DPA can be evaluated.

Conclusion

This study shows that t-MA, DPA, and canals associated with them have a lot of variations. The most common morphological variation related to these arterial structures in both PPF and GPC is the distal branching pattern. 3DRA imaging provides valuable information especially in vascular anatomical studies, as it allows submillimetric evaluation and detailed measurements. In this regard, radiological studies can guide surgery through preoperatively determining landmarks. Further studies are needed to define these topographical or radiological landmarks that might reduce the complications rates related to procedures performed at the PPF and GPC level.

Author contributions IIOZ: protocol/project development, data collection or management, data analysis, manuscript writing/editing. AA: data analysis, data collection or management, manuscript writing/editing. TFY: data collection or management, data analysis, manuscript writing/editing.

Declarations

Conflict of interests The authors declare that they have no known competing financial interests or personal relationships that could have appeared to influence the work reported in this paper.

References

1. Al-Shouk AAA-HM, Tatar İ (2021) The blood supply of the inferior nasal concha (turbinate): a cadaveric anatomical study. Anat Sci Int 96:13–19. https://doi.org/10.1007/s12565-020-00552-0
2. Apinhasmit W, Chompoopong S, Methathrathip D, Sangvichien S, Karuwanarint S (2005) Clinical anatomy of the posterior maxilla pertaining to Le Fort I osteotomy in Thais. Clin Anat 18:323–329. https://doi.org/10.1002/ca.20131
3. Assam JH, Quinn TH, Militsakh ON (2017) The maxillary artery as a recipient vessel option for complex midface and anterior skull base microsurgical repair: a cadaveric study. Microsurgery 37:611–617. https://doi.org/10.1002/micr.30095
4. Awad AS, Tohamy HMA, Gadallah HN, Ibrahim MEE-D, Raafat TA (2020) Role of multi-detector CT in analysis of the greater and lesser palatine foramina. Egypt J Radiol Nucl Med 51:150. https://doi.org/10.1186/s43055-020-00272-5
5. Bahşi İ, Orhan M, Kervancıoğlu P, Yalçın ED (2019) Morphometric evaluation and clinical implications of the greater palatine foramen, greater palatine canal and pterygopalatine fossa on CBCT images and review of literature. Surg Radiol Anat 41:551–567. https://doi.org/10.1007/s00276-019-02179-x
6. Cagimni P, Govsa F, Ozer MA, Kazak Z (2017) Computerized analysis of the greater palatine foramen to gain the palatine neurovascular bundle during palatal surgery. Surg Radiol Anat 39:177–184. https://doi.org/10.1007/s00276-016-1691-0
7. Choi J, Park HS (2003) The clinical anatomy of the maxillary artery in the pterygopalatine fossa. J Oral Maxillofac Surg 61:72–78. https://doi.org/10.1053/joms.2003.50012
8. D'Souza AS, Mamatha H, Jyothi N (2012) Morphometric analysis of hard palate in south Indian skulls. Biomed Res 23:173–175
9. Hassanali J, Mwaniki D (1984) Palatal analysis and osteology of the hard palate of the Kenyan African skulls. Anat Rec 209:273–280. https://doi.org/10.1002/ar.1092090213
10. Jotania B, Patel S, Patel S, Patel P, Patel S, Patel K (2013) Morphometric analysis of hard palate. Int J Res Med 2:72–75
11. Klosek SK, Rungruang T (2009) Anatomical study of the greater palatine artery and related structures of the palatal vault: considerations for palate as the subepithelial connective tissue graft donor site. Surg Radiol Anat 31:245–250. https://doi.org/10.1007/s00276-008-0432-4
12. Kwak HH, Jo JB, Hu KS, Oh CS, Koh KS, Chung IH, Kim HJ (2010) Topography of the third portion of the maxillary artery via the transantral approach in Asians. J Craniofac Surg 21:1284–1289. https://doi.org/10.1097/SCS.0b013e3181e1b33c
13. Lee HY, Kim HU, Kim SS, Son EJ, Kim JW, Cho NH, Kim KS, Lee JG, Chung IH, Yoon JH (2002) Surgical anatomy of the sphenopalatine artery in lateral nasal wall. Laryngoscope 112:1813–1818. https://doi.org/10.1097/00005537-200210000-00020
14. MacArthur FJ, McGarry GW (2017) The arterial supply of the nasal cavity. Eur Arch Otorhinolaryngol 274:809–815
15. Miwa Y, Asaumi R, Kawai T, Maeda Y, Sato I (2018) Morphological observation and CBCT of the bony canal structure of the groove and the location of blood vessels and nerves in the palatine of elderly human cadavers. Surg Radiol Anat 40:199–206. https://doi.org/10.1007/s00276-017-1952-6
16. Morton AL, Khan A (1991) Internal maxillary artery variability in the pterygopalatine fossa. Otolaryngol Head Neck Surg 104:204–209. https://doi.org/10.1177/019459989110400208
17. Mostafa BE, Elsamny TA, Youssef TA, Elserwi AB, Teaima AA (2018) Arterial blood supply of the nose: an angiographic study. J Otorhinolaryngol Relat Spec 80:238–247. https://doi.org/10.1159/000490254
18. Neruntarat C (2007) Uvulopalatal flap. In: Kountakis SE, Önerci M (eds) Rhinologic and sleep apnea surgical techniques. Springer, Heidelberg, pp 309–314
19. Odabaşı O, Erkmen E, ÖzlemÜçok C, AkifBakir M, YıldızerKeriş E, Şahin O (2021) Morphometric analysis of pterygomaxillary region by using cone beam computed tomography. J Stomatol Oral Maxillofac Surg 122:273–277. https://doi.org/10.1016/j.jormas.2020.06.006
20. Orhan M, Midilli R, Gode S, Saylam CY, Karci B (2010) Blood supply of the inferior turbinate and its clinical applications. Clin Anat 23:770–776. https://doi.org/10.1002/ca.21019
21. Osborn AG (1979) Radiology of the pterygoid plates and pterygopalatine fossa. Am J Roentgenol 132:389–394
22. Padgham N, Vaughan-Jones R (1991) Cadaver studies of the anatomy of arterial supply to the inferior turbinates. J R Soc Med 84:728–730
23. Scott JR, Psaltis AJ, Wormald P-J (2020) Vascular anatomy of the inferior turbinate and its clinical implications. Am J Rhinol Allergy 34:604–609
24. Standring S (2016) Gray's anatomy : the anatomical basis of clinical practice. Elsevier Limited, New York
25. Tashi S, Purohit BS, Becker M, Mundada P (2016) The pterygopalatine fossa: imaging anatomy, communications, and pathology revisited. Insights Imaging 7:589–599. https://doi.org/10.1007/s13244-016-0498-1
26. Touré G (2019) Distribution of the maxillary artery in the deep regions of the face and the maxilla: clinical applications. J Plast Reconstr Aesthet Surg 72:1020–1024. https://doi.org/10.1016/j.bjps.2019.02.008
27. Ueki K, Hashiba Y, Marukawa K, Nakagawa K, Okabe K, Yamamoto E (2009) Determining the anatomy of the descending palatine artery and pterygoid plates with computed tomography in Class III patients. J Craniomaxillofac Surg 37:469–473. https://doi.org/10.1016/j.jcms.2009.03.010
28. Uysal II, Buyukmumcu M, Dogan NU, Seker M, Ziylan T (2011) Clinical significance of maxillary artery and its branches: a cadaver study and review of the literature. Int J Morphol 29:1274–1281